Title

Atomic-scale in situ observation of electron beam and heat induced crystallization of Ge nanoparticles and transformation of Ag@Ge core-shell nanocrystals

Journal

The Journal of Chemical Physics, 158(16)

ISSN

0021-9606

Authors

Qi, Xiao

Bustillo, Karen C

Kauzlarich, Susan M

Publication Date

2023-04-28

DOI

10.1063/5.0144742

Peer reviewed

The Journal of Chemical Physics

RESEARCH ARTICLE | APRIL 24 2023

Atomic-scale *in situ* observation of electron beam and heat induced crystallization of Ge nanoparticles and transformation of Ag@Ge core-shell nanocrystals

Special Collection: 40 Years of Colloidal Nanocrystals in JCP

Xiao Qi ; Karen C. Bustillo ; Susan M. Kauzlarich

J. Chem. Phys. 158, 164704 (2023)
https://doi.org/10.1063/5.0144742

The Journal of Chemical Physics ARTICLE scitation.org/journal/jcp

Atomic-scale *in situ* observation of electron beam and heat induced crystallization of Ge nanoparticles and transformation of Ag@Ge core-shell nanocrystals

Cite as: J. Chem. Phys. 158, 164704 (2023); doi: 10.1063/5.0144742
Submitted: 31 January 2023 • Accepted: 10 April 2023 •
Published Online: 24 April 2023

Xiao Qi,[1] Karen C. Bustillo,[2] and Susan M. Kauzlarich[1,a)]

AFFILIATIONS

[1] Department of Chemistry, University of California, Davis, California 95616, USA
[2] National Center for Electron Microscopy, Molecular Foundry, Lawrence Berkeley National Laboratory, Berkeley, California 94720, USA

Note: This paper is part of the JCP Special Topic on 40 Years of Colloidal Nanocrystals in JCP.
[a)] **Author to whom correspondence should be addressed:** smkauzlarich@ucdavis.edu

ABSTRACT

Crystallization of amorphous materials by thermal annealing has been investigated for numerous applications in the fields of nanotechnology, such as thin-film transistors and thermoelectric devices. The phase transition and shape evolution of amorphous germanium (Ge) and Ag@Ge core–shell nanoparticles with average diameters of 10 and 12 nm, respectively, were investigated by high-energy electron beam irradiation and *in situ* heating within a transmission electron microscope. The transition of a single Ge amorphous nanoparticle to the crystalline diamond cubic structure at the atomic scale was clearly demonstrated. Depending on the heating temperature, a hollow Ge structure can be maintained or transformed into a solid Ge nanocrystal through a diffusive process during the amorphous to crystalline phase transition. Selected area diffraction patterns were obtained to confirm the crystallization process. In addition, the thermal stability of Ag@Ge core–shell nanoparticles with an average core of 7.4 and a 2.1 nm Ge shell was studied by applying the same beam conditions and temperatures. The results show that at a moderate temperature (e.g., 385 °C), the amorphous Ge shell can completely crystallize while maintaining the well-defined core–shell structure, while at a high temperature (e.g., 545 °C), the high thermal energy enables a freely diffusive process of both Ag and Ge atoms on the carbon support film and leads to transformation into a phase segregated Ag–Ge Janus nanoparticle with a clear interface between the Ag and Ge domains. This study provides a protocol as well as insight into the thermal stability and strain relief mechanism of complex nanostructures at the single nanoparticle level with atomic resolution.

INTRODUCTION

The properties of nanocrystals are highly dependent on their composition, structure, and morphology. Tailored synthesis with control of these parameters can be successfully applied to produce nanocrystals with the desired properties for specific applications. In recent years, low-dimensional Ge structures have received significant attention because of their superior electrical and optical properties, which enable the fabrication of high-performance devices including plasmonics,[1] photodetectors,[2–4] multi-junction solar cells,[5,6] lithium–ion batteries,[7–9] and nano-optoelectronic devices.[10] To further enhance their performance, a variety of metals have been thermally introduced into Ge-based nanowires to fabricate reliable metal-semiconductor heterostructures.[11–17] However, most studies focus on the fabrication of 1D heterojunction due to the lack of synthetic methods for high quality Ge quantum dots. Moreover, radial metal-semiconductor heterostructures are typically unstable due to the strain induced by the large lattice mismatch. Such 0D metal-semiconductor heterostructures are rarely reported in the literature.

The synthesis of Ag@Ge metal-semiconductor core–shell heterostructures with highly controllable shell thickness via an unconventional galvanic replacement reaction was reported.[18] Considering the different atomic radii and different crystal lattices

(Ag is face-centered cubic and Ge is diamond cubic), strain is expected at the Ag@Ge core–shell interface. Therefore, investigating the thermal stability and strain relief mechanism of such 0D metal-semiconductor heterostructures is vital to understand their formation mechanism, optimize the synthesis condition, and prevent mechanical failure in industrial applications.

The thermal history of a nanoparticle system contributes to its morphology and structure. Consecutive heating via rapid thermal annealing is a common technique to study the thermal stability of nanomaterials. Traditional methods include heating powder in a tube furnace or heating mantle, followed by characterization using X-ray diffraction (XRD) to study the phase transformation conditions. However, due to the high surface energy, the phase transition temperature is highly dependent on the size and morphology of the nanomaterial, which makes the precise determination of the phase transition temperature for specific nanostructures extremely challenging. For example, the crystallization of amorphous Ge nanoparticles investigated by *in situ* XRD was found to occur between 550 and 600 °C.[19] However, *in situ* TEM showed that above 480 °C, small Ge nanoparticles (2–3 nm) become non-crystalline, while nanoparticles greater than 5 nm remain crystalline.[20]

The thermal stability of a metal/semiconductor interface has also been studied by many groups. For example, platinum (Pt) thermal diffusion into a silicon (Si) nanowire to create a Pt–Si contact has been reported.[21] However, such a diffusion process is highly dependent on the homogeneity and quality of the nanowires and is thus hard to reproduce.[22] There is a large body of work examining metal induced crystallization of diamond cubic semiconductor thin films, for example, in the recent work by Kryshtal *et al.*,[23] specific to the Ag–Ge system. The previous metal-induced crystallization report suggests that a minimum amount of Ge, more than what is present in the 2 nm Ge shell in this current work, is required for such metal-induced transformation. In this current work, the eutectic liquid required to sustain crystallization is not present.

Compared to the traditional methods discussed earlier, *in situ* TEM, as reported by Mongillo *et al.*,[24] is another powerful tool to study an all-solid-state reaction activated by conventional thermal heating. Since the nanoparticles are permanently fixed on the supporting carbon film of the TEM grid, it is possible to observe the phase transition process of a single nanoparticle at high resolution. Moreover, because the Ge nanoparticles are well separated from each other by their surface ligands, the packing density can be easily controlled by the concentration of nanoparticles. Mutual diffusion and dispersion between adjacent nanoparticles can be prohibited so that the all-solid-state interface diffusion process, as well as the accompanying morphological changes, can be better studied. Many of the observations in this work are specific to the proximity of a thermally conductive support.

Here, real-time observations of the dynamic crystallization process for both hollow and solid amorphous Ge nanoparticles obtained through a combination of *in situ* sample heating and high-energy electron beams by TEM are presented. In parallel, the thermal stability and structural evolution of the Ag@Ge core–shell nanostructure are revealed at the atomic level. By combining real-time structural imaging with elemental analysis, the transformation process is shown to occur through the crystallization of the amorphous Ge shell accompanied by surface segregation of Ag.

RESULTS AND DISCUSSION

Synthesis of amorphous Ge and Ag@Ge core–shell nanoparticles

Galvanic replacement is a versatile strategy to prepare hollow metallic nanostructures by substituting one metal with another metal with a higher reduction potential.[25] While many synthetic strategies have been explored to fine-tune the reaction kinetics, such as introducing a competitive reducing agent or substituting the metal precursor,[26–29] solid and core–shell nanostructures via electrical displacement are rarely reported due to the low energy barrier and fast reaction rate even at 0 °C.[30–34]

In contrast, by controlling the solubility and mobility of Ge free ions via a combination of different organic ligands, temperature, and precursor molar ratios, amorphous Ge nanoparticles can be synthesized via galvanic replacement in high boiling-point organic solvents.[18] A detailed synthesis method is included in the supplementary material. Figure 1 shows the high-angle annular dark-field scanning transmission electron microscopy (HAADF-STEM) images of the as-synthesized amorphous Ge solids and hollow nanoparticles. The average diameters of the solid and hollow Ge nanoparticles are 7.3 ± 0.4 nm and 9.3 ± 0.4 nm, respectively. It is worth noting that, since the electrochemical reaction of such galvanic replacement is mostly localized within a single particle, the size distribution of the final product cannot be effectively converged by classical nucleation and growth theories, such as LaMer nucleation theory[35] and Ostwald ripening.[36] Although the complete galvanic replacement between Ag and Ge makes it feasible to produce pure non-hollow Ge nanoparticles at a moderate reaction temperature, prolonged local ion diffusion would cause the destruction of the original particle morphology and form some random shapes, as shown in the supplementary material, Fig. S1. Such random shapes are not conducive to the orderly arrangement of nanoparticles when drop-cast onto the TEM grid and introduce undesirable mutual diffusion and dispersion between the adjacent nanoparticles. Since our study focused on the single particle level, we chose the synthetic conditions in order to obtain quasi-spherical Ge nanoparticles. These synthetic conditions inevitably introduced some Ag–Ge core–shell intermediate structures on the same TEM grid, which are visible in the center particle of Fig. 1(a), which has a much brighter Ag core.

Structural and compositional characterizations of Ag@Ge core–shell nanoparticles

A unique Ag@Ge core–shell nanostructure can be well-separated as an intermediate by moderate synthesis temperature and fast quenching. The annular bright-field and simultaneously recorded HAADF-STEM images, as shown in Fig. 2, reveal that the nanocrystals have a well-defined core–shell configuration with a distinct interface. The high brightness of the core is due to the high Z nucleus (Z = 47) and the crystalline structure of the Ag; the Ge shell has lower intensity scattering due to the lower Z (Z = 32) nucleus and its amorphous structure. It is important to mention that, due to the phase contrast nature of TEM mode, the amorphous Ge shell is hardly visible at higher magnification, especially on a relatively thick (15 nm) amorphous carbon support (an example is shown in the supplementary material, Fig. S2), and thus all the HRTEM data in this study were collected at a certain defocus value to increase the

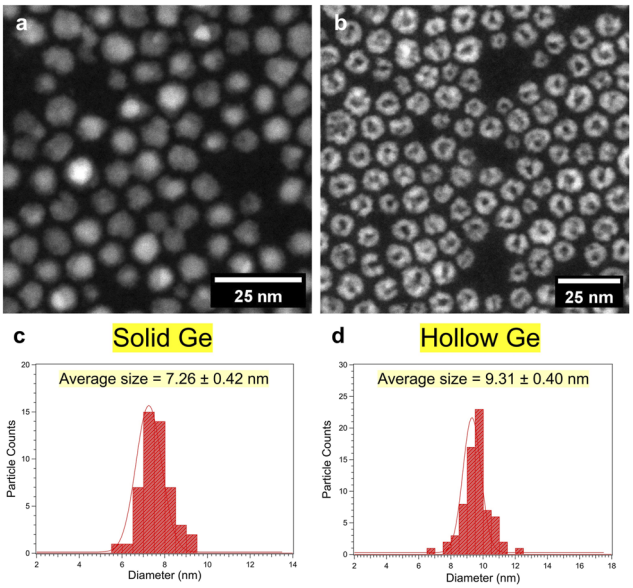

FIG. 1. HAADF-STEM images of the solid (a) and hollow (b) Ge nanoparticles. The HAADF-STEM collection angle is 55 mrad. The much brighter spots in (a) show a small amount of unreacted Ag core in the Ag@Ge intermediate due to synthesis conditions, while the hollow Ge in (b) is the result of a complete galvanic replacement reaction between Ag nanoparticles and GeI_2 at a much faster rate. Size histogram of solid Ge (c) and hollow Ge (d) show the average diameters of the solid and hollow Ge nanoparticles are 7.3 ± 0.4 nm and 9.3 ± 0.4 nm, respectively.

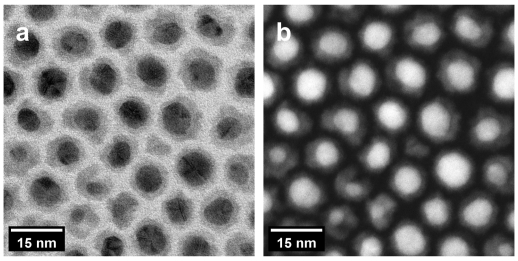

FIG. 2. Annular bright-field (ABF)-STEM and corresponding HAADF-STEM images of Ag@Ge core–shell nanocrystals.

image contrast. To characterize the composition and elemental distribution of the nanoparticles, we carried out a detailed analysis by energy dispersive spectrometry (EDS). As shown from the elemental maps in Fig. 3, the core area of the nanoparticle mainly shows the signal of Ag, in line with the structural analysis. In contrast, the shells are mainly composed of Ge. The corresponding EDS spectrum is shown in the supplementary material, Fig. S3, and a separate EDS spectrum exclusively collected at the Ge shell area is shown in the supplementary material, Fig. S4. The oxygen percentage is much higher on the blank carbon support (O: Ge = 9:1) than on the Ge shell region (1:2.4), indicating that the oxygen signal is more likely to come from the TEM grid rather than the Ge shell.

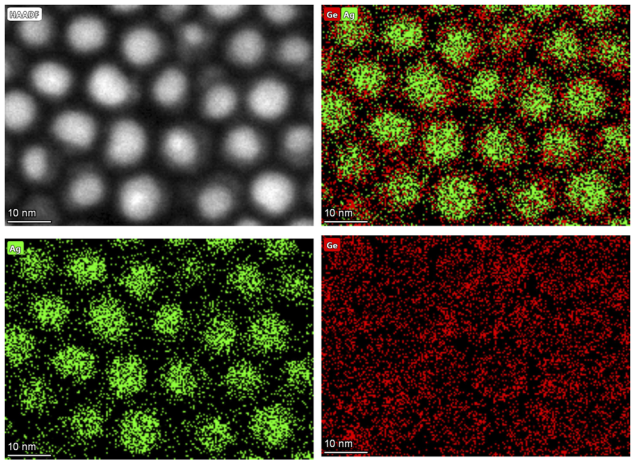

FIG. 3. HAADF-STEM image and corresponding elemental maps of Ag and Ge from their L and K edges, respectively.

In situ observation of the crystallization of amorphous solid Ge nanoparticles

The crystallization of amorphous Ge nanoparticles was observed during *in situ* heating TEM experiments with an annealing process aimed at mapping out the structural evolution during the entire crystallization process and investigating the phase change temperature. Convincing imaging of the Ge nanoparticles using the TEM mode is challenging because the focus of the microscope inevitably changes due to the thermal drift of the sample during the *in situ* heating process in a conventional furnace-based heating holder. As a result, resolution deteriorates due to drifting during the image recording. To this end, the specimen was preheated to a certain temperature, and then a focused electron beam induced the crystallization and restructuring of the Ge nanoparticles. This approach of using the 300 kV e-beam to both probe and modify the particle allowed for the investigation of the crystallization of a single amorphous Ge nanoparticle *in situ* and at the atomic scale. At room temperature, the Ge nanoparticle was largely amorphous. The specimen was gradually heated to 385 °C until it started to show evidence of crystallization, as shown in the first frame in Fig. 4. The electron beam was blanked, and the temperature was maintained at 385 °C until no thermal vibration of the specimen could be detected. Then the beam was condensed to maintain a screen current of 6.24 nA and a dose rate of 1.38×10^5 e/Å^{2}s resulting in the complete crystallization of amorphous Ge within 5 min, as shown in Fig. 4. The top-left corner of the amorphous Ge nanoparticle shows some lattice fringes at time 00:00. Then, crystallization nucleated from the existing crystalline site, and after 5 min, the Ge nanoparticle transformed into a crystalline nanoparticle. The whole series was collected with some objective lens defocus to increase image contrast, and the movie is provided in the supplementary material, Movie S1. Analysis of the FFT image of the last frame (supplementary material, Fig. S5) indicates a d-spacing of 0.33 nm for the 111 reflection of the diamond cubic lattice of Ge, which agrees with the known value of 0.3266 nm. Notice that even though the whole specimen was maintained at 385 °C for about 1 h, the other Ge nanoparticles outside

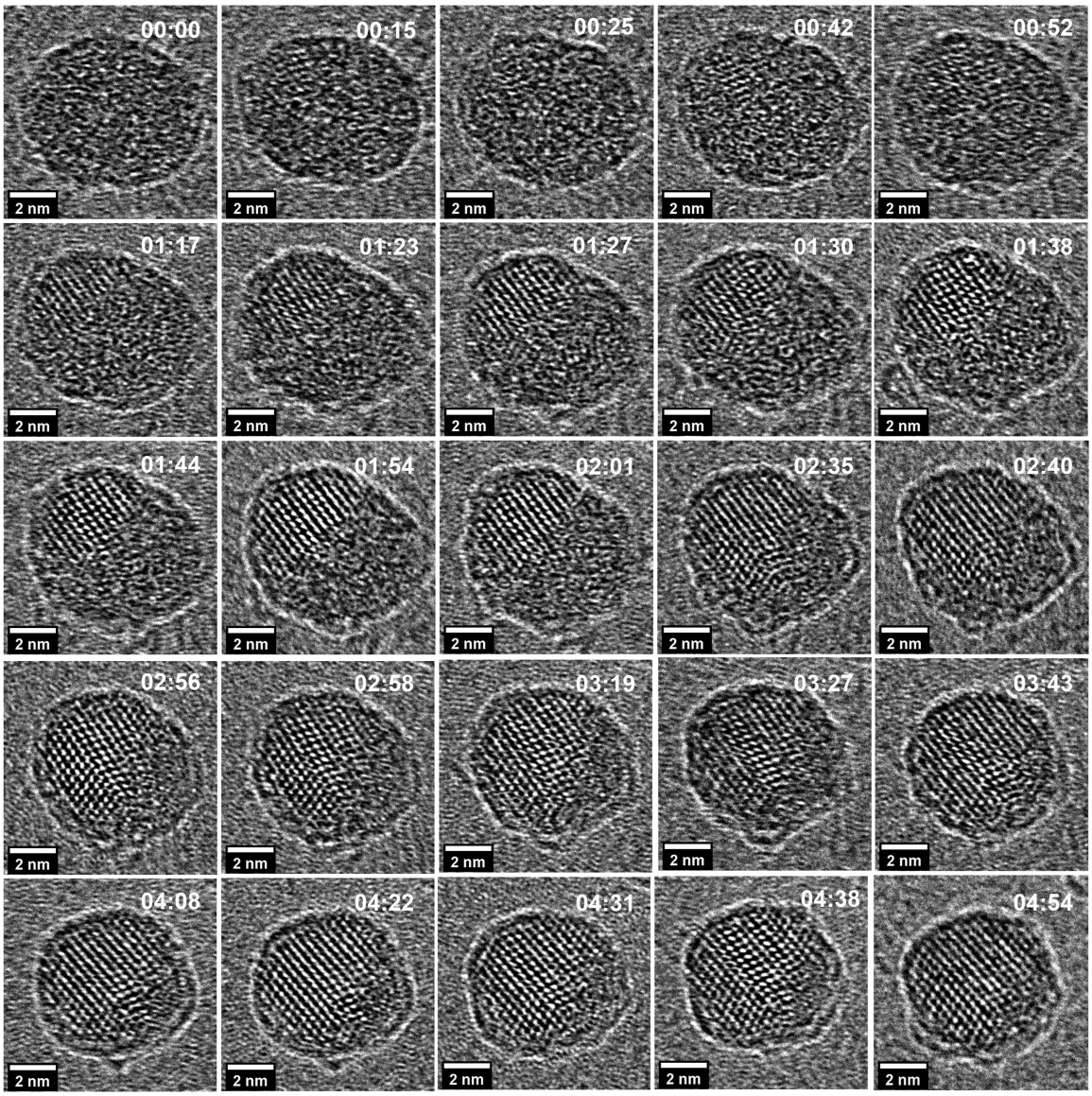

FIG. 4. *In situ* observation of crystallization of an amorphous solid Ge nanoparticle.

the viewing field remained amorphous. This indicates that the phase transformation temperature for the nanoparticles on this support was higher than 385 °C; however, the 300 kV electron beam provided the additional energy to induce the crystallization process. After a further increase in temperature to 545 °C, all the amorphous Ge nanoparticles were transformed into crystalline Ge without the help of the electron beam. In addition, selected area electron diffraction (SAED) data were collected with an aperture defining a region of interest with a diameter of about 1 μm during the crystallization process, further confirming that the crystallization temperature was above 385 °C, as shown in Fig. 5.

In situ observation of the crystallization of amorphous hollow Ge

The same approach was applied to the amorphous hollow Ge nanoparticles to study the crystallization process. Figure 6(a) shows a typical bright-field TEM image of the as-synthesized hollow Ge nanoparticles. After the heating started, the image drifted due to the thermal expansion of the metallic TEM grid, as shown in Fig. 6(b). After the temperature stabilized at 385 °C for about 1 h, the drift was minimized, and a high-resolution TEM image of the hollow Ge nanoparticles was obtained, as shown in Fig. 6(c). At 385 °C,

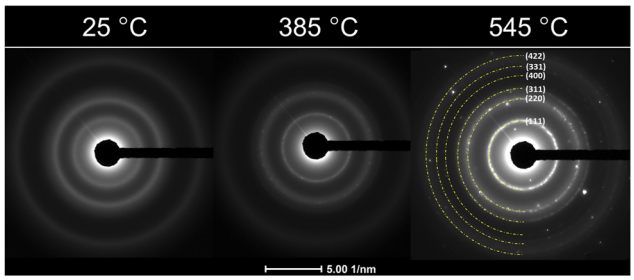

FIG. 5. Selected area electron diffraction (SAED) pattern of the Ge nanoparticles at (a) 25 °C, (b) 385 °C, and (c) 545 °C. The diffraction pattern of crystalline Ge on the right was indexed to be (111), (220), (311), (400), (331), and (422) planes of diamond cubic Ge.

the hollow Ge nanoparticles started the diffusion process, as indicated by the change in morphology of the hollow Ge nanoparticles over time as the Ge nanoparticles coalesce. However, the hollow Ge nanoparticle appears to be amorphous, which further indicates that the temperature is below the crystallization temperature. As the temperature was increased further to 545 °C, the amorphous Ge nanoparticles crystallized, as shown in Fig. 6(d). Clear lattice fringes can be observed in the image. At this temperature, the Ge atoms had gained enough energy to diffuse and reorganize into a more thermally stable configuration, and in many cases, the pinhole of the hollow Ge nanoparticles close to minimize the surface energy. This results in the conversion of the hollow structure into a solid

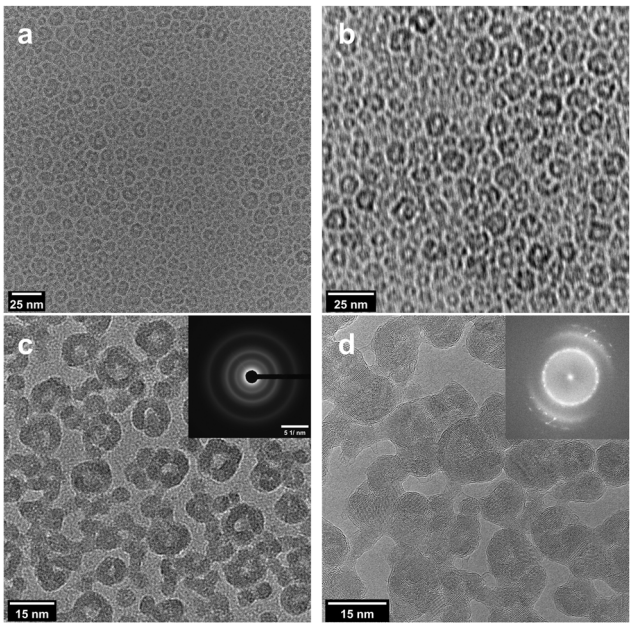

FIG. 6. (a) TEM image of the synthesized hollow Ge nanoparticles. (b) TEM recorded during the *in situ* heating process; resolution is impacted by the thermal drift of the sample. (c) The amorphous hollow Ge nanoparticles at 385 °C. The inset is the diffraction pattern of the TEM image from a region of 1 μm in diameter. (d) The hollow Ge nanoparticles show crystallization at 545 °C. The inset is the corresponding FFT image.

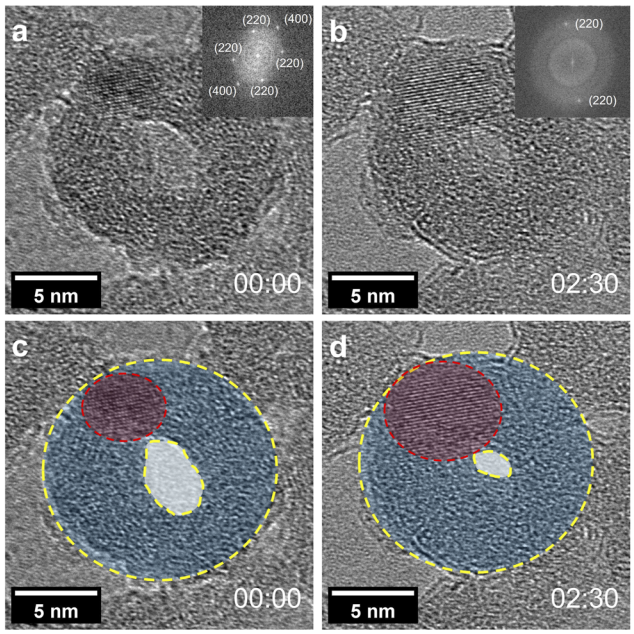

FIG. 7. *In situ* observation of crystallization of amorphous hollow Ge nanoparticles. TEM images of a single hollow Ge nanoparticle time-stamped at 00:00 (a) and 02:30 (b) after the electron beam was initially turned on. The temperature was maintained at 385 °C during the observation period. The FFTs corresponding to the crystalline regions are shown as insets. (c) and (d) are the same TEM images as (a) and (b), but with colored regions of amorphous hollow Ge (blue) and crystalline Ge grains (red).

crystalline Ge nanoparticle. As a second example, Fig. 7 shows an *in situ* observation of the partial crystallization of a single amorphous hollow Ge nanoparticle under the 300 kV electron beam at 385 °C. Notice that the hollow shape was initially maintained, and the crystallized area increased as more high-energy electrons impinged on the nanoparticles. The expansion of the crystallized area can be clearly seen in Figs. 7(c) and 7(d). The FFT confirms the d-spacing of the Ge diamond cubic lattice.

In situ observation of the structural transformation of Ag@Ge core–shell nanocrystals

To investigate the heat-induced metal-semiconductor redistribution in the anisotropic hetero-nanostructure with high spatial resolution and chemical sensitivity, a heating experiment was performed using a MEMS-based *in situ* heating holder. The Ag@Ge core–shell nanocrystals were drop-cast onto a copper TEM grid with amorphous carbon support and then loaded on the heating chip of a Protochips Fusion TEM holder. It was found that the core–shell structure remained stable below 200 °C. No obvious changes were observed except that in the temperature range of 100–150 °C, carbon contamination accumulated during the imaging process because of the interaction between the surfactant and the electron beam. The carbon contamination became negligible when the temperature was above 200 °C due to the decomposition of the surfactant. With a heating rate of 5 °C/min, the temperature was increased to 385 °C, as indicated in the previous experiment. Under an e-beam with a screen current of 6.24 nA and a dose rate of 1.38 × 10^5 e/Å^{2}s, some

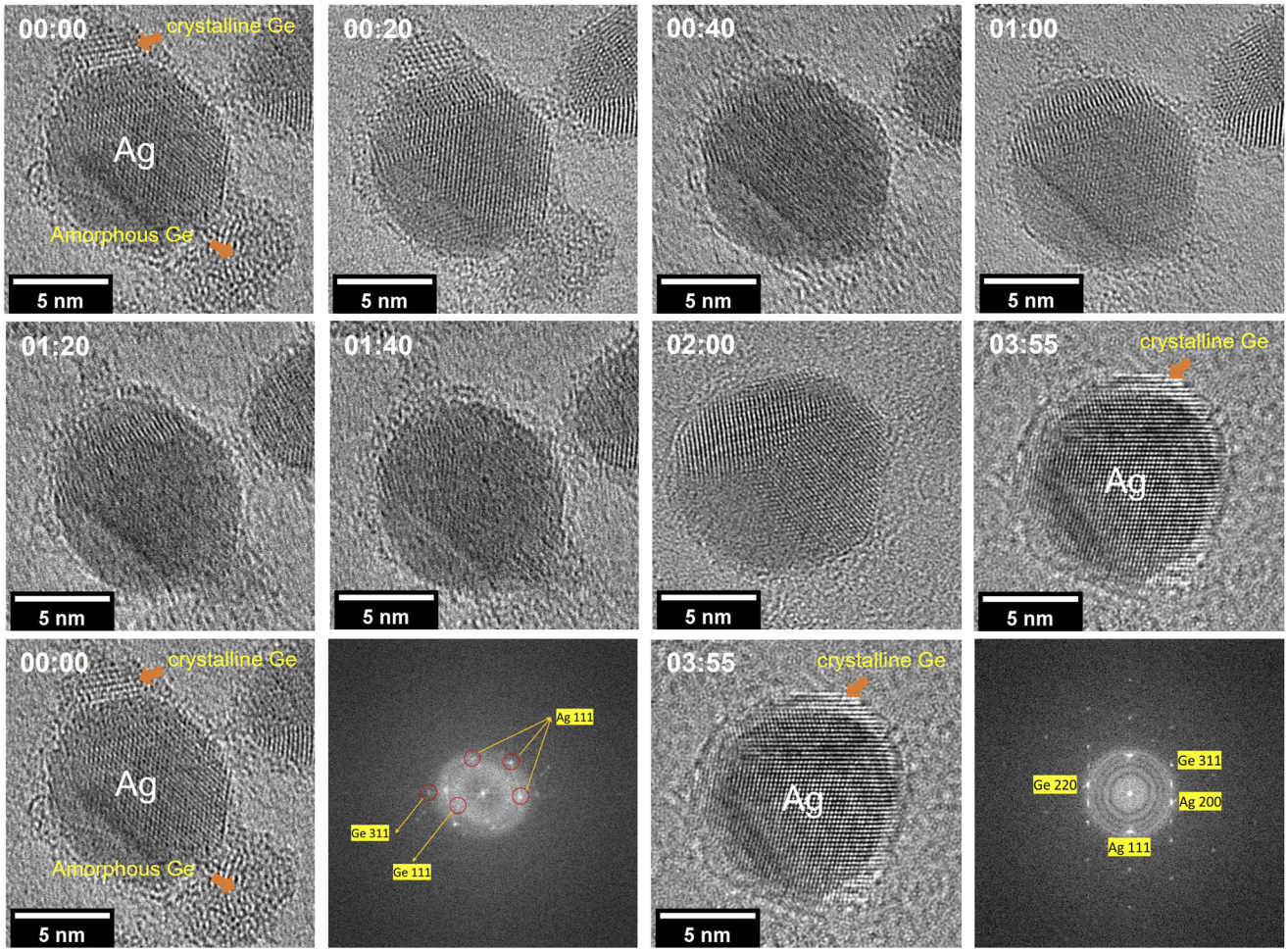

FIG. 8. Time-series of *in situ* observation of the transformation of Ag@Ge core–shell nanoparticles at 385 °C. The bottom row shows the FFT of the first and last frames to confirm the crystalline structure of the Ge and Ag domains.

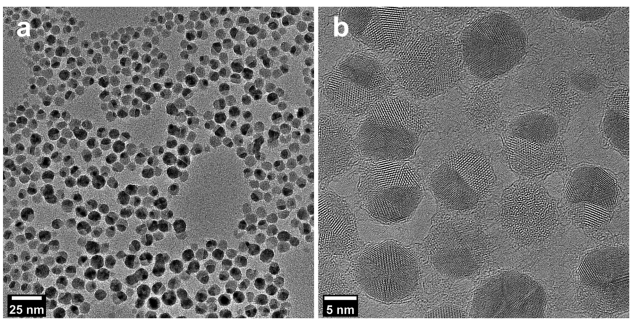

FIG. 9. TEM images of the Ag–Ge Janus nanoparticles at 545 °C at low (a) and high (b) resolution.

of the Ge shell was observed to crystallize, but the core–shell configuration remained stable. It was observed that the two different Ge domains gradually diffused to the surface of the Ag core and merged and reconstructed on the surface, forming a uniform crystalline Ge layer that covered the Ag core with a sharp heterointerface between, as shown in Fig. 8. It is also noted that, after the first 2 min, the Ge shell remained amorphous. However, during the next 2 min, the strong electron beam facilitated the formation of crystalline Ge.

In contrast, when the temperature was further increased to 545 °C, Ag@Ge core–shell nanoparticles were transformed into Janus Ag–Ge nanoparticles with two distinct phases, as shown in Fig. 9. This transformation is attributed to the high interface energy between the core and the shell. The high energy of the Ag–Ge interface compared with either the Ge or Ag surface is minimized in this configuration, where the shared interface is nearly a straight line. Figure 10 clearly shows such a transformation within a single Ag@Ge core–shell nanoparticle. At 545 °C, the Ag atoms gained enough energy to diffuse on the amorphous carbon support of the TEM grid. Therefore, the core–shell nanostructures transformed into Janus particles to minimize the interface between the Ag and Ge domains and reduce the overall free energy. A video of the transformation process is included in the supplementary material, Movie S2.

Typically, core–shell nanoparticles are synthesized based on the atomic size, relative strengths of homonuclear bonds, and surface energies of elements.[37] In most cases, the smaller atomic size element resides in the core, while the larger atomic-size element comprises the shell due to steric constraints. However, once exposed to high annealing temperatures, the surface energy dictates the diffusion of the element either from the core or shell.[38] Core–shell nanoparticles from completely soluble solid systems such as Au–Pd[39] and Co–Pt[40] are well studied and show that homogeneous structures form after thermal annealing, while heterodimers or nanohybrid structures are to be expected in bimetallic systems with immiscible and lattice-mismatched elements due to interfacial strain minimization during thermal induction.[41–44] Our study shows that metal-semiconductor core–shell nanostructures with even higher interfacial strain transform from a well-defined core–shell nanostructure into a heterodimer.

CONCLUSION

Using TEM, we have investigated the structure and phase transformation of both amorphous Ge and Ag@Ge nanoparticles. By holding the sample temperature below the crystallization temperature for the Ge nanoparticles, we were able to use the electron beam to initiate the crystallization slowly enough that TEM images document the phase transformation. The thermal

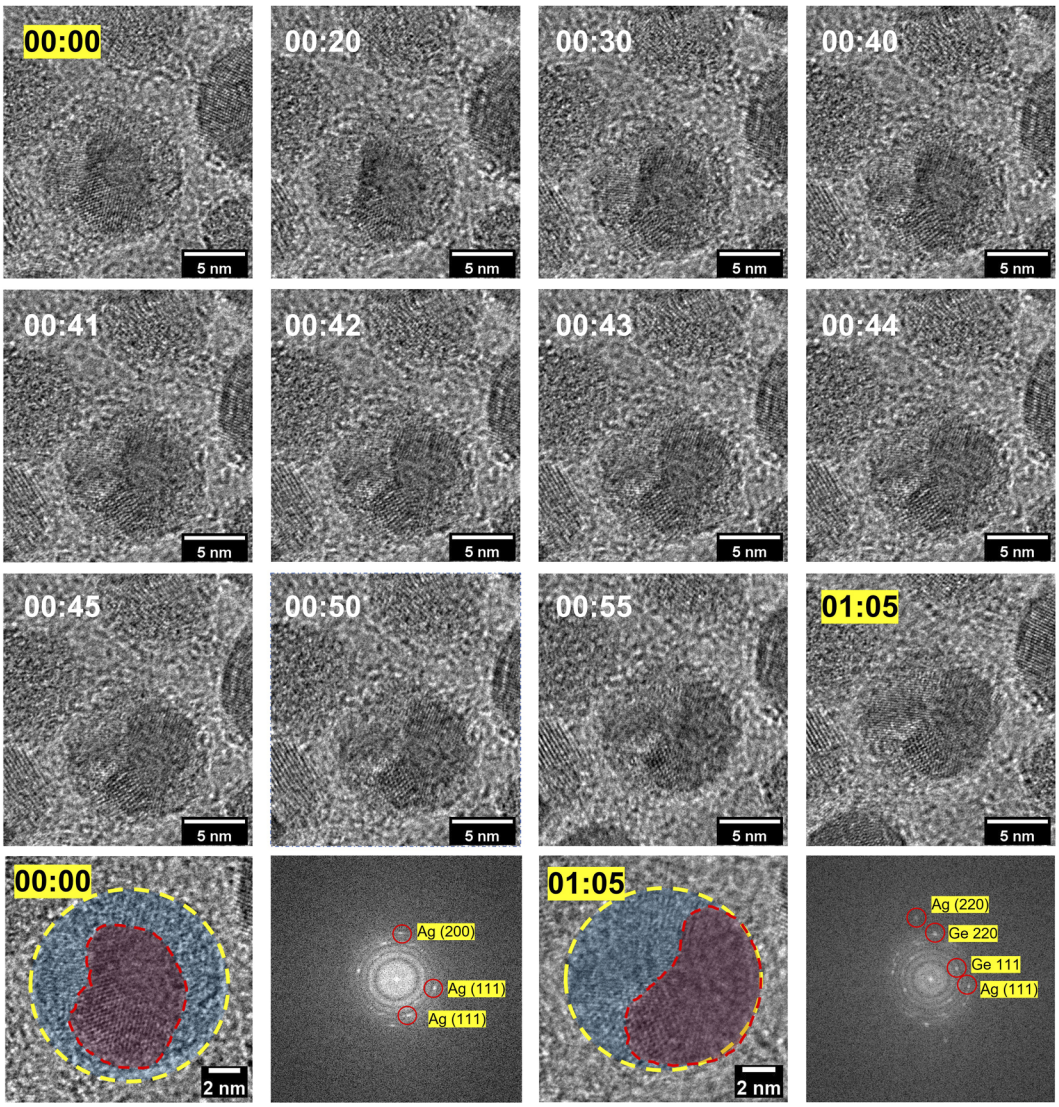

FIG. 10. Time-series of *in situ* observation of the transformation of a single Ag@Ge core–shell nanoparticle into an Ag–Ge heterodimer at 545 °C. Ag domain and Ge domain are color-coded in the first frame and last frame to show Ag diffusion to the edge of the core–shell nanoparticle. The corresponding FFT clearly shows the crystalline planes of Ag in the first frame and both Ag and Ge in the last frame.

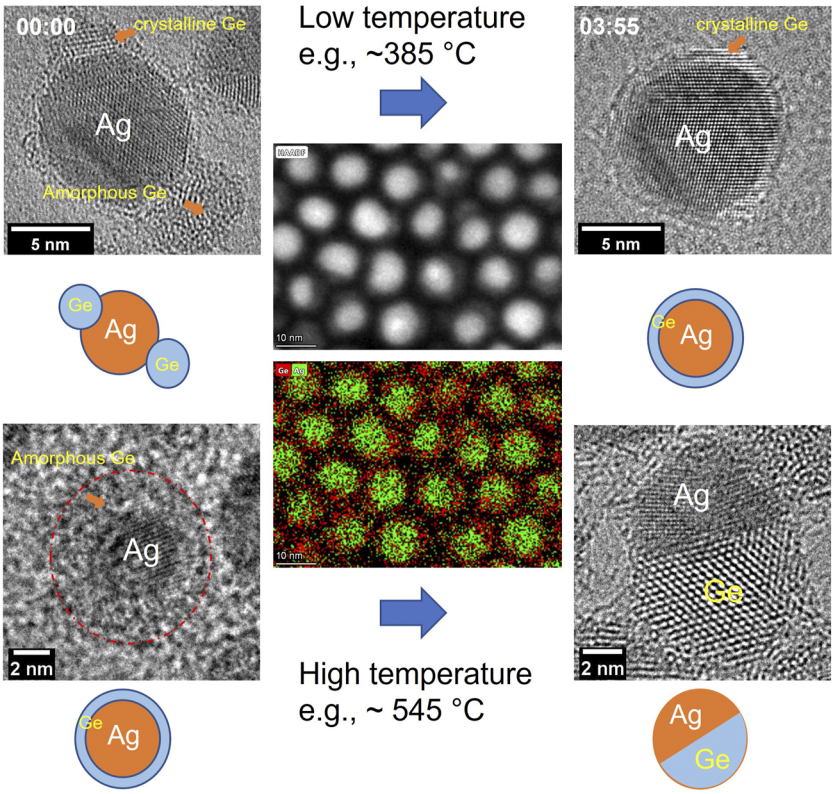

FIG. 11. Scheme of the morphologic and crystallinity transformations of Ag@Ge core–shell nanoparticles at different temperatures. EDS mapping in the center shows the Ag@Ge core–shell nanostructure. At a moderate temperature (e.g., 385 °C), the Ag@Ge core–shell nanostructure can be maintained while the amorphous Ge shell crystallized under the synergistic effect of heat and a high energy electron beam, as shown both in the TEM image and cartoon on the top panel. At a higher temperature (e.g., 545 °C), further heating enabled the diffusive process of both Ag and Ge atoms leading to the transformation of the core–shell nanostructure into a phase segregated Ag–Ge Janus nanoparticle, as shown on the bottom panel.

behavior of Ag@Ge core–shell nanostructures was also explored under similar heating and electron beam conditions. At a moderate temperature, the amorphous Ge shell crystallized while maintaining the core–shell nanostructure. Furthermore, heating enabled the diffusive process of both Ag and Ge atoms leading to the transformation of the core–shell nanostructure into a phase segregated Ag–Ge Janus nanoparticle with a clear interface between the Ag and Ge domains. The transformation process is summarized in Fig. 11. The synergistic effect of heat and an electron beam allows for imaging of the thermal stability and strain relief mechanism of complex nanostructures with high surface tension and lattice strains at the single nanoparticle level with high resolution. This method could be adapted to study other nanostructures such as metal alloys, metal-semiconductor hetero nanostructures, and doped nanomaterials.

SUPPLEMENTARY MATERIAL

See the supplementary material for the dynamic process in Fig. 4 (Movie S1) and Fig. 10 (Movie S2) (avi). Materials and Methods, a TEM image of Ge nanoparticles synthesized at 150 °C, a series of TEM images of Ge nanoparticles recorded at different magnifications and defocus values, EDS spectra from Fig. 3, and the last TEM frame of Fig. 4 (PDF).

ACKNOWLEDGMENTS

This work was supported by the National Science Foundation under Grant No. CHE-1710110. Electron microscopy at the Molecular Foundry was supported by the Office of Science, Office of Basic Energy Sciences, of the U.S. Department of Energy under Contract No. DE-AC02-05CH11231. We acknowledge Dr. Andrew Thron from the Advanced Materials Characterization and Testing Laboratory (AMCaT) at UC Davis for his help with TEM and STEM measurements and useful discussions.

AUTHOR DECLARATIONS

Conflict of Interest

The authors have no conflicts to disclose.

Author Contributions

Xiao Qi: Conceptualization (equal); Formal analysis (equal); Investigation (equal); Methodology (equal); Validation (equal); Writing – original draft (equal); Writing – review & editing (equal). **Karen C. Bustillo**: Methodology (equal); Supervision (equal); Writing – review & editing (supporting). **Susan M. Kauzlarich**: Conceptualization (lead); Funding acquisition (lead); Project administration (lead); Supervision (lead); Writing – review & editing (lead).

DATA AVAILABILITY

The data that support the findings of this study are available within the article.

REFERENCES

[1]L. Baldassarre, E. Sakat, J. Frigerio, A. Samarelli, K. Gallacher, E. Calandrini, G. Isella, D. J. Paul, M. Ortolani, and P. Biagioni, "Midinfrared plasmon-enhanced spectroscopy with germanium antennas on silicon substrates," Nano Lett. **15**(11), 7225–7231 (2015).

[2]L. Tang, S. E. Kocabas, S. Latif, A. K. Okyay, D.-S. Ly-Gagnon, K. C. Saraswat, and D. A. B. Miller, "Nanometre-scale germanium photodetector enhanced by a near-infrared dipole antenna," Nat. Photonics **2**(4), 226–229 (2008).

[3]S. Assefa, F. Xia, and Y. A. Vlasov, "Reinventing germanium avalanche photodetector for nanophotonic on-chip optical interconnects," Nature **464**(7285), 80–84 (2010).

[4]J. Michel, J. Liu, and L. C. Kimerling, "High-performance Ge-on-Si photodetectors," Nat. Photonics **4**(8), 527–534 (2010).

[5]W. Guter, J. Schöne, S. P. Philipps, M. Steiner, G. Siefer, A. Wekkeli, E. Welser, E. Oliva, A. W. Bett, and F. Dimroth, "Current-matched triple-junction solar cell reaching 41.1% conversion efficiency under concentrated sunlight," Appl. Phys. Lett. **94**(22), 223504 (2009).

[6]R. R. King, D. C. Law, K. M. Edmondson, C. M. Fetzer, G. S. Kinsey, H. Yoon, R. A. Sherif, and N. H. Karam, "40% efficient metamorphic GaInP/GaInAs/Ge multijunction solar cells," Appl. Phys. Lett. **90**(18), 183516 (2007).

[7]M.-H. Park, Y. Cho, K. Kim, J. Kim, M. Liu, and J. Cho, "Germanium nanotubes prepared by using the Kirkendall effect as anodes for high-rate lithium batteries," Angew. Chem., Int. Ed. **50**(41), 9647–9650 (2011).

[8]W. Li, M. Li, Z. Yang, J. Xu, X. Zhong, J. Wang, L. Zeng, X. Liu, Y. Jiang, X. Wei, L. Gu, and Y. Yu, "Carbon-coated germanium nanowires on carbon nanofibers as self-supported electrodes for flexible lithium-ion batteries," Small **11**(23), 2762–2767 (2015).

[9]S. Wu, C. Han, J. Iocozzia, M. Lu, R. Ge, R. Xu, and Z. Lin, "Germanium-based nanomaterials for rechargeable batteries," Angew. Chem., Int. Ed. **55**(28), 7898–7922 (2016).

[10]Y.-T. Wu, C.-W. Huang, C.-H. Chiu, C.-F. Chang, J.-Y. Chen, T.-Y. Lin, Y.-T. Huang, K.-C. Lu, P.-H. Yeh, and W.-W. Wu, "Nickel/platinum dual silicide axial nanowire heterostructures with excellent photosensor applications," Nano Lett. **16**(2), 1086–1091 (2016).

[11]N. S. Dellas, S. Minassian, J. M. Redwing, and S. E. Mohney, "Formation of nickel germanide contacts to Ge nanowires," Appl. Phys. Lett. **97**(26), 263116 (2010).

[12]B. Liu, Y. Wang, S. Dilts, T. S. Mayer, and S. E. Mohney, "Silicidation of silicon nanowires by platinum," Nano Lett. **7**(3), 818–824 (2007).

[13]T. Burchhart, A. Lugstein, Y. J. Hyun, G. Hochleitner, and E. Bertagnolli, "Atomic scale alignment of copper-germanide contacts for Ge nanowire metal oxide field effect transistors," Nano Lett. **9**(11), 3739–3742 (2009).

[14]S. A. Dayeh, N. H. Mack, J. Y. Huang, and S. T. Picraux, "Advanced core/multishell germanium/silicon nanowire heterostructures: The Au-diffusion bottleneck," Appl. Phys. Lett. **99**(2), 023102 (2011).

[15]Y.-C. Chou, W.-W. Wu, S.-L. Cheng, B.-Y. Yoo, N. Myung, L. J. Chen, and K. N. Tu, "In-situ TEM observation of repeating events of nucleation in epitaxial growth of nano $CoSi_2$ in nanowires of Si," Nano Lett. **8**(8), 2194–2199 (2008).

[16]T. Izumi, M. Taniguchi, S. Kumai, and A. Sato, "Ferromagnetic properties of cyclically deformed Fe_3Ge and Ni_3Ge," Philos. Mag. **84**(36), 3883–3895 (2004).

[17]M. Jamet, A. Barski, T. Devillers, V. Poydenot, R. Dujardin, P. Bayle-Guillemaud, J. Rothman, E. Bellet-Amalric, A. Marty, J. Cibert, R. Mattana, and S. Tatarenko, "High-Curie-temperature ferromagnetism in self-organized $Ge_{1-x}Mn_x$ nanocolumns," Nat. Mater. **5**(8), 653–659 (2006).

[18]X. Qi and S. M. Kauzlarich, "Ge nanocages and nanoparticles via microwave-assisted galvanic replacement for energy storage applications," ACS Appl. Nano Mater. **3**(6), 5509–5520 (2020).

[19]H. W. Chiu, C. N. Chervin, and S. M. Kauzlarich, "Phase changes in Ge nanoparticles," Chem. Mater. **17**(19), 4858–4864 (2005).

[20]H. W. Chiu, S. M. Kauzlarich, and E. Sutter, "Thermal behavior and film formation from an organogermanium polymer/nanoparticle precursor," Langmuir **22**(12), 5455–5458 (2006).

[21]Y.-C. Lin, K.-C. Lu, W.-W. Wu, J. Bai, L. J. Chen, K. N. Tu, and Y. Huang, "Single crystalline PtSi nanowires, PtSi/Si/PtSi nanowire heterostructures, and nanodevices," Nano Lett. **8**(3), 913–918 (2008).

[22]Y. E. Yaish, A. Katsman, G. M. Cohen, and M. Beregovsky, "Kinetics of nickel silicide growth in silicon nanowires: From linear to square root growth," J. Appl. Phys. **109**(9), 094303 (2011).

[23]A. Kryshtal, S. Bogatyrenko, and P. Ferreira, "Metal-induced crystallization of amorphous semiconductor films: Nucleation phenomena in Ag-Ge films," Appl. Surf. Sci. **606**, 154873 (2022).

[24]M. Mongillo, P. Spathis, G. Katsaros, P. Gentile, M. Sanquer, and S. De Franceschi, "Joule-assisted silicidation for short-channel silicon nanowire devices," ACS Nano **5**(9), 7117–7123 (2011).

[25]M. H. Oh, T. Yu, S.-H. Yu, B. Lim, K.-T. Ko, M.-G. Willinger, D.-H. Seo, B. H. Kim, M. G. Cho, J.-H. Park, K. Kang, Y.-E. Sung, N. Pinna, and T. Hyeon, "Galvanic replacement reactions in metal oxide nanocrystals," Science **340**(6135), 964–968 (2013).

[26]C. Gao, Z. Lu, Y. Liu, Q. Zhang, M. Chi, Q. Cheng, and Y. Yin, "Highly stable silver nanoplates for surface plasmon resonance biosensing," Angew. Chem., Int. Ed. **51**(23), 5629–5633 (2012).

[27]Y. Yang, J. Liu, Z.-W. Fu, and D. Qin, "Galvanic replacement-free deposition of Au on Ag for core–shell nanocubes with enhanced chemical stability and SERS activity," J. Am. Chem. Soc. **136**(23), 8153–8156 (2014).

[28]M. M. Shahjamali, M. Bosman, S. Cao, X. Huang, S. Saadat, E. Martinsson, D. Aili, Y. Y. Tay, B. Liedberg, S. C. J. Loo, H. Zhang, F. Boey, and C. Xue, "Gold coating of silver nanoprisms," Adv. Funct. Mater. **22**(4), 849–854 (2012).

[29]R. G. Sanedrin, D. G. Georganopoulou, S. Park, and C. A. Mirkin, "Seed-mediated growth of bimetallic prisms," Adv. Mater. **17**(8), 1027–1031 (2005).

[30]Y. Sun, B. Mayers, and Y. Xia, "Metal nanostructures with hollow interiors," Adv. Mater. **15**(7-8), 641–646 (2003).

[31]S. E. Skrabalak, L. Au, X. Li, and Y. Xia, "Facile synthesis of Ag nanocubes and Au nanocages," Nat. Protoc. **2**(9), 2182–2190 (2007).

[32]D. Seo and H. Song, "Asymmetric hollow nanorod formation through a partial galvanic replacement reaction," J. Am. Chem. Soc. **131**(51), 18210–18211 (2009).

[33]M. McEachran, D. Keogh, B. Pietrobon, N. Cathcart, I. Gourevich, N. Coombs, and V. Kitaev, "Ultrathin gold nanoframes through surfactant-free templating of faceted pentagonal silver nanoparticles," J. Am. Chem. Soc. **133**(21), 8066–8069 (2011).

[34]X. Hong, D. Wang, S. Cai, H. Rong, and Y. Li, "Single-crystalline octahedral Au–Ag nanoframes," J. Am. Chem. Soc. **134**(44), 18165–18168 (2012).

[35]V. K. LaMer and R. H. Dinegar, "Theory, production and mechanism of formation of monodispersed hydrosols," J. Am. Chem. Soc. **72**(11), 4847–4854 (1950).

[36]W. Ostwald, "Über die vermeintliche Isomerie des roten und gelben Queck-silberoxyds und die," Oberflächenspannung fester Körper **34U**(1), 495–503 (1900).

[37]R. Ferrando, J. Jellinek, and R. L. Johnston, "Nanoalloys: From theory to applications of alloy clusters and nanoparticles," Chem. Rev. **108**(3), 845–910 (2008).

[38]P. Lu, M. Chandross, T. J. Boyle, B. G. Clark, and P. Vianco, "Equilibrium Cu-Ag nanoalloy structure formation revealed by in situ scanning transmission electron microscopy heating experiments," APL Mater. **2**(2), 022107 (2014).

[39]Y. Ding, F. Fan, Z. Tian, and Z. L. Wang, "Atomic structure of Au–Pd bimetallic alloyed nanoparticles," J. Am. Chem. Soc. **132**(35), 12480–12486 (2010).

[40]J.-Y. Bigot, H. Kesserwan, V. Halté, O. Ersen, M. S. Moldovan, T. H. Kim, J.-t. Jang, and J. Cheon, "Magnetic properties of annealed core–shell CoPt nanoparticles," Nano Lett. **12**(3), 1189–1197 (2012).
[41]A. O. Yalcin, B. de Nijs, Z. Fan, F. D. Tichelaar, D. Vanmaekelbergh, A. van Blaaderen, T. J. H. Vlugt, M. A. van Huis, and H. W. Zandbergen, "Core–shell reconfiguration through thermal annealing in FexO/$CoFe_2O_4$ ordered 2D nanocrystal arrays," Nanotechnology **25**(5), 055601 (2014).
[42]W. Liu, K. Sun, and R. Wang, "In situ atom-resolved tracing of element diffusion in NiAu nanospindles," Nanoscale **5**(11), 5067–5072 (2013).
[43]J. Yang and J. Y. Ying, "Diffusion of gold from the inner core to the surface of Ag_2S nanocrystals," J. Am. Chem. Soc. **132**(7), 2114–2115 (2010).
[44]T. Mokari, A. Aharoni, I. Popov, and U. Banin, "Diffusion of gold into InAs nanocrystals," Angew. Chem., Int. Ed. **45**(47), 8001–8005 (2006).